Femur Bone Implant Plate Design Analysis Under Varying Fracture Conditions

Nilesh Tipan, Ajay Pandey, and Girish Chandra

1 Introduction

The femur bone is the most proximal bone in human beings that plays a prominent role in daily activities like walking, running and jumping [1, 2]. In human anatomy, femur is the longest and largest bone, but it is strong enough only for compressive loads [3]. The femur is responsible for supporting the highest percentage of body weight during normal exercise. The femur body is long, thin and almost cylindrical in structure. Bone fracture of femur is one of the most common traumas. Femoral fractures are quite problematic and responsible for significant orthopedic trauma because they are the strongest, longest and heaviest bones in the human body [4, 5]. Femoral shaft fractures in human beings occur frequently due to high-power collisions that are typical of road accidents, fall from a height, gunshot wounds, etc. A relatively low-intensity accident, such as fall from standing position, can also create a femoral fracture in an old person with weak bones [6].

There are three fracture regions in a femur bone fracture: the top/neck of the bone (near the pelvis), the primary shaft of the bone or the lower end near the knee. Injury happens when a high-force blow hits the thigh bone [7]. This can be due to the frame weight of the person or a collision with an object [8].

Femur fractures vary greatly, depending on the force that causes the break. The items of bone could line up properly (stable fracture) or be out of alignment (displaced fracture). The skin around the fracture could be intact (closed fracture), or the bone could puncture the skin (open fracture) [9]. Femur fractures are categorized depending on the specific fracture location (distal, center or proximal) and/or the fracture pattern (crosswise, lengthwise or concentrated toward the middle).

N. Tipan (✉) · A. Pandey · G. Chandra
Department of Mechanical Engineering, Maulana Azad National Institute of Technology, Bhopal, Madhya Pradesh 462003, India

P. Verma et al. (eds.), *Advancement in Materials, Manufacturing and Energy Engineering, Vol. I*, Lecture Notes in Mechanical Engineering,
https://doi.org/10.1007/978-981-16-5371-1_36

Bone tissue, unlike most body tissues, has the remarkable capacity to regenerate itself [10–12]. If a fractured bone can be held correctly, it may regenerate the tissue and regain most of its authentic strength [13, 14]. For intense fractures, bone plates are surgically implanted to preserve the bone at its vicinity. The design of implant plates is largely influenced by the choice of the material and its biocompatibility [15–17]. The bone plate needs to be sufficiently strong to support the weight generally transferred onto the bone, even as the bone heals. The plate ought to have additional stiffness to support the bone to which it is attached. The implant must be non-toxic and non-inflammatory [18–20].

The stiffness of the bone plate is important from the viewpoint of protection from stress generated due to stiffness differential. Strain defense is the phenomenon, wherein the implant bears maximum burden typically placed on the bone [21]. This is favorable while the bone is vulnerable. This is essentially because when the bone heals and regains power, there might be a loss in bone mass and strength is regained if the bone plate does, now, not allow the bone to carry growing load [22].

2 Materials and Methodology

2.1 Material Selection

Orthopedic applications have conventionally employed metallic alloys, like stainless steel (SS316L), titanium alloy (Ti6Al4V) and cobalt–chromium (Co–Cr) to make different elements of implants, namely the screws, plates, nails, etc. The common mechanical properties of these biomaterials and cortical bone are listed in Table 1. These are considered throughout this work. These biomaterials are observed biocompatible under physiological environments and possess adequate mechanical strength and properties.

Table 1 Mechanical properties of cortical bone and conventionally used metallic alloys

Element	Density (Kg/m^3)	Young's modulus (Gpa)	Poisson's ratio	Ultimate tensile strength (Mpa)	Ultimate compressive strength (Mpa)
Cortical bone	1750	16.7	0.3	43.44 ± 3.62	115.29 ± 12.94
SS316L	7750	193	0.31	485	570
CoCr alloy	8500	210	0.34	960	560
Ti6A14V	4512	119	0.37	1200	1080

2.2 Design of Plate and Assembly

In osteosynthesis, most fracture cases may be cured using different types of plates, namely the straight plate, cobra head plate, tabular plate, reconstruction plate, etc., and corresponding screws with buttress threads. These implants are generally made up of metallic alloys listed above. In this analysis, three different designs of plates and respective screws have been prepared with these three different biomaterials having been taken for each design, and analysis has been carried out with commonly occurring loading and boundary conditions for the fracture of femur bone as shown in Fig. 1. These designs have been successfully configured in assembly with the femoral fractured bone structure and screws with the help of computational design approaches.

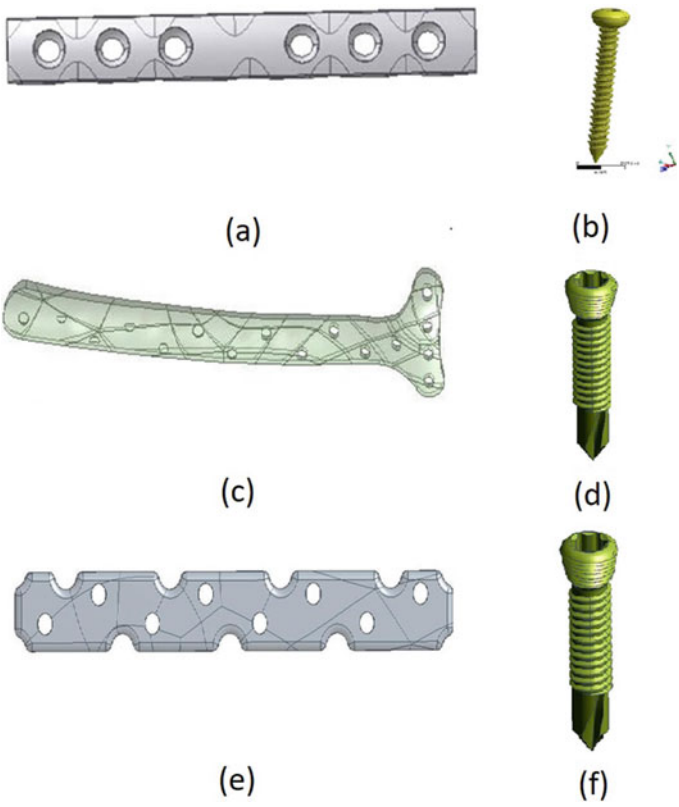

Fig. 1 Plates and screws for different design, **a** and **b** shows implant plate and screw, respectively, for Design-1 which will be used for all material combinations (i.e., stainless steel alloy, titanium alloy and chromium–cobalt alloy), **c** and **d** shows implant plate and screw, respectively, for Design-2 which will be used for all material combinations, **e** and **f** shows implant plate and screw, respectively, for Design-3 which will be used for all material combinations

2.3 Meshing

The finite element analysis reduces the degrees of freedom from infinite to finite with the help of meshing or discretization. The analysis accuracy and duration depend on the mesh size and orientation. For an optimum analysis using FEM, the implant assembly has been divided into many elements and nodes and calculations carried out at a limited number of points. The results have been extrapolated to arrive at results for the entire domain. All three designs of implant plate are shown in Fig. 2, with meshed geometry, which contains adaptive size and tetrahedral-structured elements. The mesh details for these designs are listed in Table 2.

2.4 Assumptions and Boundary Conditions

The designs of plate with assembled fractured femur have been assumed to be homogeneous in materials properties. Meshes are tetrahedral structured and adaptive in sizing for all three designs. Any structure can be tested only with specified boundary and loading conditions. In this case, a fixed support is provided at the lower part of the femur bone in such a manner that it can deform or move in all possible directions or exhibit multi-degree of freedom behavior, except the vertical downward translation. The load acting on the femur is applied on the upper part of vertically oriented femur bone with a value of ~ 750 N based on maximum average weight of human beings. For dynamic and fatigue analysis, transient structural loading is selected for the second analysis, and auto-step time of 0.1 s for each step is set. Nonlinear controls are set as default or program controlled, and the output results are noted as stresses, deformation, etc.

3 Results

According to input loading and boundary conditions, deformation, generated stress and fatigue performance of the three implant plate designs for the three materials under consideration have been observed and analyzed. The output results are listed below.

3.1 Total Deformation

The comparative analysis for all three designs is shown in Fig. 3, in terms of total deformation. It can be observed that the total deformation in case of Design-1 for SS316L varies from the minimum to moderate under the permissible range. This is

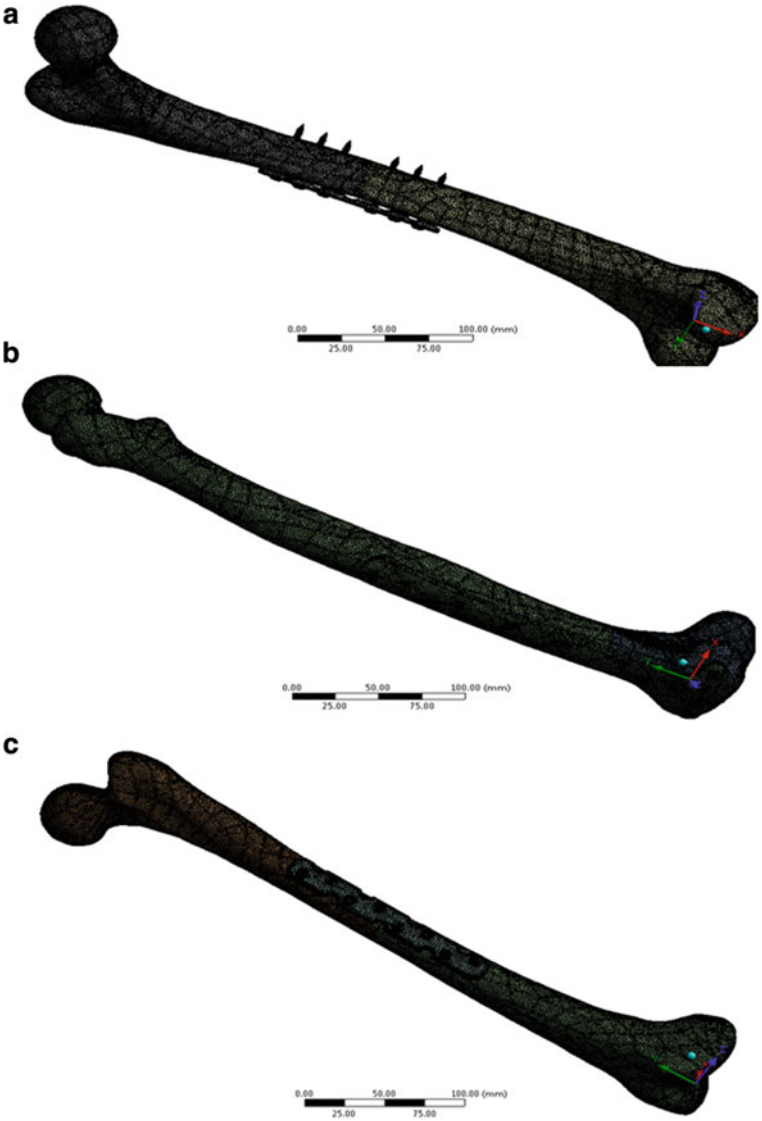

Fig. 2 Meshing of **a** plate Design-1, **b** plate Design-2 and **c** plate Design-3 with femur bone fracture

Table 2 Meshing details of three different plates assembled with respective fractured positions of femur bone

Design of plate with femur	Numbers of nodes	Number of elements
Design-1	938,820	569,821
Design-2	1,060,797	628,480
Design-3	1,393,335	866,696

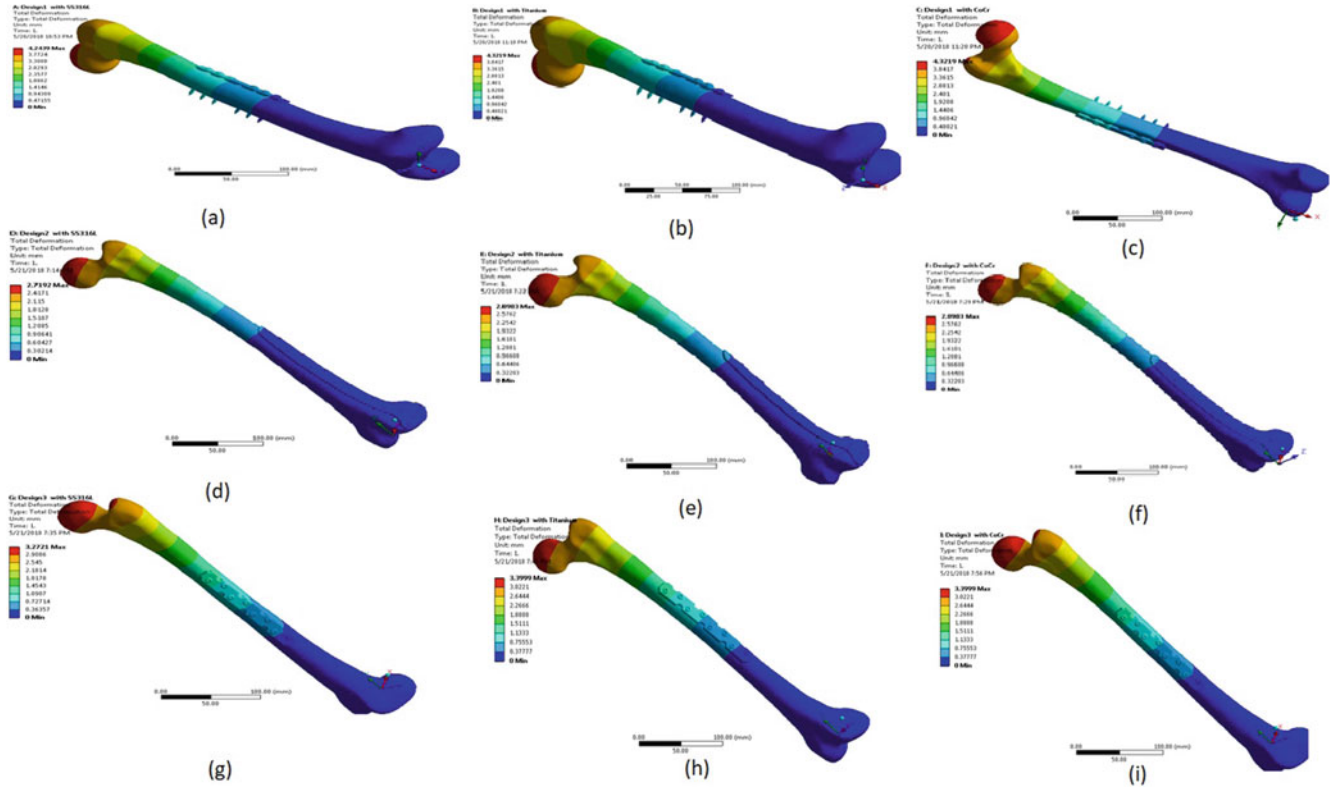

Fig. 3 Total deformation of three designs of plate with corresponding material, i.e., **a** Design-1 with stainless steel alloy **b** Design-1 with titanium alloy **c** Design-1 with CoCr alloy **d** Design-2 with stainless steel alloy **e** Design-2 with titanium alloy **f** Design-2 with CoCr alloy **g** Design-3 with stainless steel alloy **h** Design-3 with titanium alloy **i** Design-3 with CoCr alloy

shown by dark blue and light blue colors. From Design-1 with titanium alloy, it can be observed that total deformation for the implant plate lies between the minimum to moderate but is inclined toward the moderate while being still under the permissible range. This is again shown by dark blue and light blue colors. From Design-1 with CoCr alloy, it can be observed that total deformation for the implant plate is inclined even more toward the moderate value in the permissible range and is shown by light blue colors.

From Design-2 with SS316L, it can be observed that total deformation is between the minimum to a moderate value but more inclined toward the minimum value which is under permissible range and is shown by dark blue and light blue colors. From Design-2 with titanium alloy, it can be observed that total deformation for the implant plate is between the minimum to a moderate value but more toward the minimum value which is under permissible range and is shown by dark blue and light blue colors. From Design-2 with CoCr alloy, it can be observed that the total deformation for the implant plate is toward the minimum value which is under permissible range and is shown by dark blue color.

From Design-3 with SS316L, it can be observed that total deformation for the implant plate varies from minimum to moderate value but is more toward the moderate value which is under permissible range and is shown by dark blue and light blue colors. From Design-3 with titanium alloy, it can be observed that total deformation for the implant plate is between the minimum to moderate value but more toward a moderate value which is under permissible range and is shown by dark blue and light blue colors. From Design-3 with CoCr alloy, it can be observed that total deformation for the implant plate is more toward a moderate value which is under permissible range and is shown by light blue color.

After performing analysis on femur bone plate using different materials and different designs, the final results obtained are shown in Table 3.

In Design-1, total deformation using different materials follows similar patterns. In Design-2, total deformation values for chromium–cobalt alloy follow a different pattern but follows a similar kind of pattern for titanium alloy and stainless steel alloy. In Design-3, values for chromium–cobalt alloy follow a different pattern, but for titanium alloy and stainless steel alloy, a similar kind of pattern is observed.

3.2 Maximum Equivalent Stress

The comparative analysis for all three designs is shown in Fig. 4, in terms of maximum equivalent stress.

It can be seen that from Design-1 with SS316L alloy, it can be observed that maximum equivalent stress for the implant plate is toward the minimum value which is under permissible range and is shown by dark blue color. From Design-1 with titanium alloy, it can be observed that maximum equivalent stress for the implant plate is toward the minimum value which is under permissible range and is shown by dark blue color. From Design-1 with CoCr alloy, it can be observed that

Table 3 Total deformation

Time	Design-1 SS316L	Design-1 Titanium alloy	Design-1 CoCr alloy	Design-2 SS316L	Design-2 Titanium alloy	Design-2 CoCr alloy	Design-3 SS316L	Design-3 Titanium alloy	Design-3 CoCr alloy
0.1	0.42241	0.43009	0.43009	0.27204	0.28993	0.28993	0.32723	0.34	0.34
0.2	0.84482	0.86019	0.86019	0.54401	0.57977	0.57977	0.65444	0.67999	0.67999
0.3	1.2672	1.2903	1.2903	0.81617	0.86981	0.86981	0.98165	1.02	1.02
0.4	1.6896	1.7204	1.7204	1.0882	1.1597	1.1597	1.3089	1.36	1.36
0.5	2.112	2.1513	2.1513	1.3602	1.45	1.45	1.6361	1.7	1.7
0.6	2.5351	2.583	2.583	1.6317	1.7397	1.7397	1.9633	2.0399	2.0399
0.7	2.959	3.0152	3.0152	1.9034	2.0293	2.0293	2.2905	2.3799	2.3799
0.8	3.3838	3.4482	3.4482	2.1752	2.3187	2.3187	2.6177	2.7199	2.7199
0.9	3.8114	3.8884	3.8884	2.447	2.6086	2.6086	2.9449	3.0599	3.0599
1	4.2439	4.3219	4.3219	2.7192	2.8983	2.8983	3.2721	3.3999	3.3999

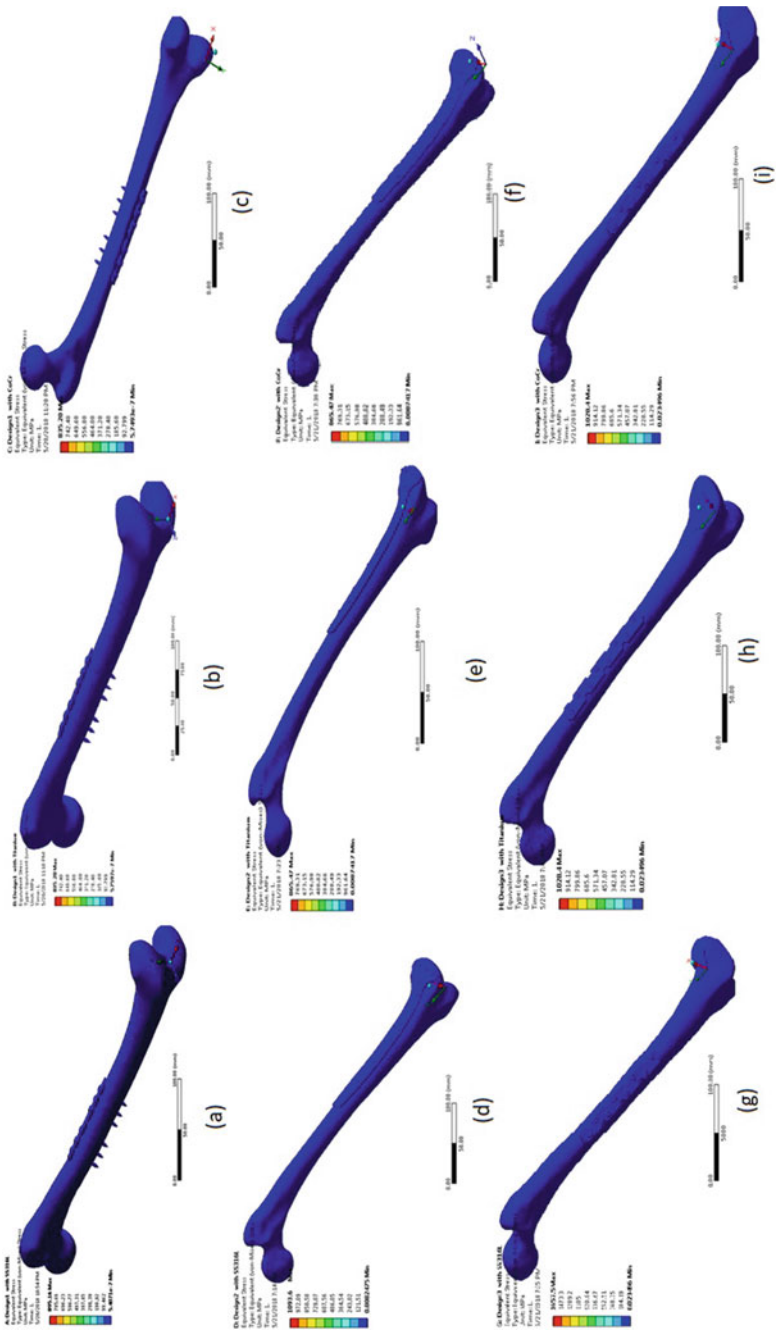

Fig. 4 Maximum equivalent stress of three designs of plate with its correspondingly used materials, i.e., **a** Design-1 with stainless steel alloy **b** Design-1 with titanium alloy **c** Design-1 with CoCr alloy **d** Design-2 with stainless steel alloy **e** Design-2 with titanium alloy **f** Design-2 with CoCr alloy **g** Design-3 with stainless steel alloy **h** Design-3 with titanium alloy **i** Design-3 with CoCr alloy

maximum equivalent stress on implant plate is toward the minimum value which is under permissible range and is shown by dark blue color.

From Design-2 with SS316L alloy, it can be observed that maximum equivalent stress is toward the minimum value which is under permissible range and is shown by dark blue color. From Design-2 with titanium alloy, it can be observed that the maximum equivalent stress for the implant plate is toward the minimum value which is under permissible range and is shown by dark blue color. From Design-2 with CoCr alloy, it can be observed that the maximum equivalent stress for the implant plate is inclined toward the minimum value which is under permissible range and is shown by dark blue color.

From Design-3 with SS316L alloy, it can be observed that maximum equivalent stress for the implant plate is toward the minimum value which is under permissible range and is shown by dark blue color. From Design-3 with titanium alloy, it can be observed that the maximum equivalent stress for the implant plate is toward the minimum value which is under permissible range and is shown by dark blue color. From Design-3 with CoCr alloy, it can be observed that maximum equivalent stress for the implant plate is toward the minimum value which is under permissible range and is shown by dark blue color.

After performing analysis on femur bone plate using different materials and different designs, the final results obtained are shown in Table 4.

In Design-1, the maximum equivalent stress using different materials follows similar patterns. In Design-2, maximum equivalent stress values for chromium–cobalt alloy follow different patterns but for titanium alloy and stainless steel alloy follow similar kind of pattern. In Design-3, values of maximum equivalent stress for chromium cobalt follow a different pattern, but for titanium alloy and stainless steel alloy, a similar kind of pattern is observed.

3.3 Maximum Principal Stress

The comparative analysis for all three designs is shown in Fig. 5, in terms of maximum principal stress. It can be seen that from Design-1with SS316L alloy, it can be observed that maximum principal stress for the implant plate is between the minimum to moderate value which is under permissible range and is shown by light blue color. From Design-1 with titanium alloy, it can be observed that the maximum principal stress for the implant plate is between the minimum and moderate which is under permissible range and is shown by light blue color. From Design-1 with CoCr alloy, it can be observed that the maximum principal stress for the implant plate is between the minimum to moderate which is under permissible range and is shown by light blue color.

From Design-2 with SS316L alloy, it can be observed that the maximum principal stress for the implant plate is between the moderate and the maximum value but inclined more toward the maximum value which is shown by dark yellow color. From Design-2 with titanium alloy, it can be observed that the maximum

Table 4 Maximum equivalent stress

Time	Design-1 SS316L	Design-1 Titanium alloy	Design-1 CoCr alloy	Design-2 SS316L	Design-2 Titanium alloy	Design-2 CoCr alloy	Design-3 SS316L	Design-3 Titanium alloy	Design-3 CoCr alloy
0.1	153.02	135.92	135.92	70.613	50.012	50.012	162.71	100.43	100.43
0.2	305.17	271.41	271.41	1558	1091.8	1091.8	328.9	203.54	203.54
0.3	457.32	406.9	406.9	27,089	20,427	20,427	494.81	306.5	306.5
0.4	609.49	542.4	542.4	57,658	43,536	43,536	660.77	409.51	409.51
0.5	761.66	14,142	14,142	43,903	38,442	38,442	826.78	512.56	512.56
0.6	15,503	23,186	23,186	44,353	45,117	45,117	992.84	615.65	615.65
0.7	24,896	24,408	24,408	1.04E+05	52,292	52,292	1158.9	718.78	718.78
0.8	58,199	84,057	84,057	84,341	52,315	52,315	1325.1	821.95	821.95
0.9	89,408	83,450	83,450	94,305	84,082	84,082	1491.3	925.15	925.15
1	89,516	83,520	83,520	1.09E+05	86,547	86,547	1657.5	1028.4	1028.4

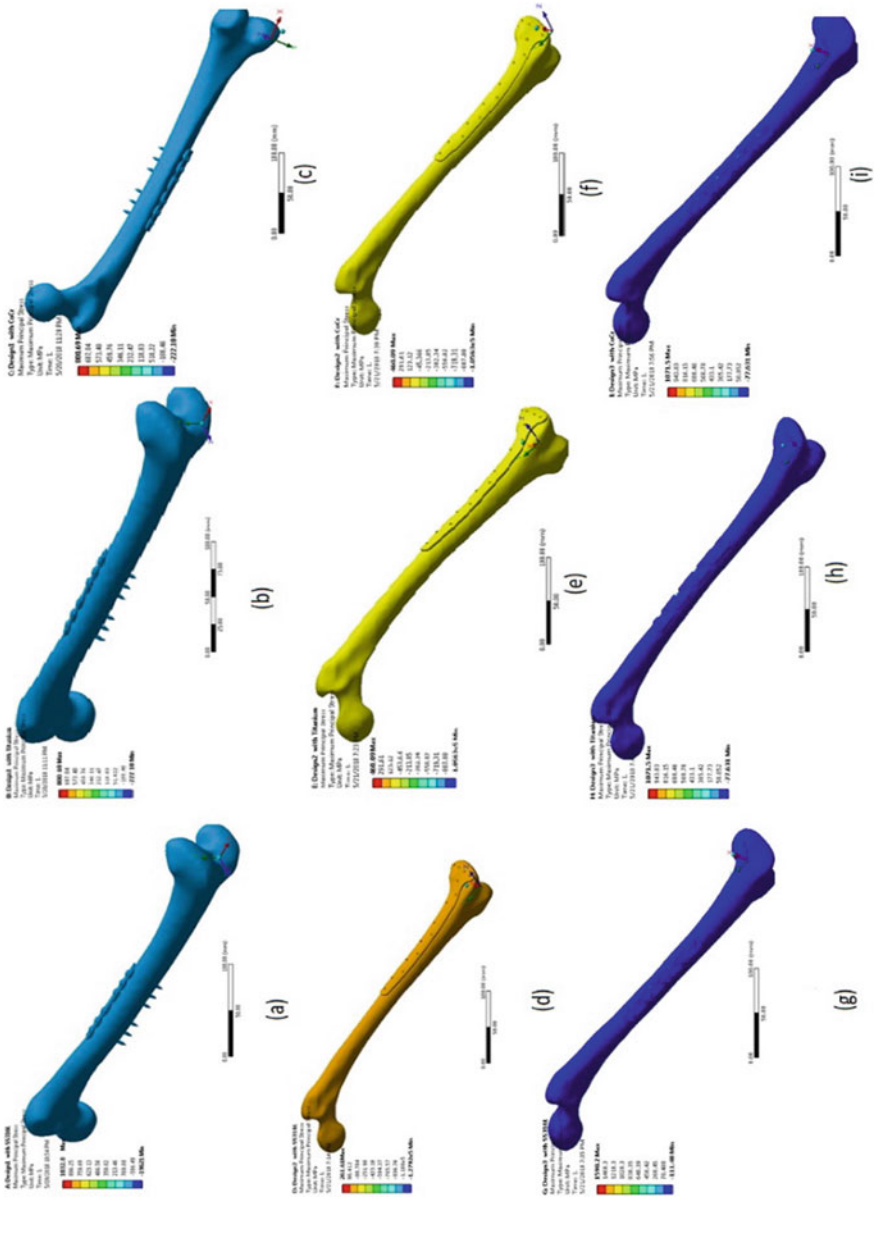

Fig. 5 Maximum principal stress of three designs of plate with its correspondingly used materials, i.e., **a** Design-1 with stainless steel alloy **b** Design-1 with titanium alloy **c** Design-1 with CoCr alloy **d** Design-2 with stainless steel alloy **e** Design-2 with titanium alloy **f** Design-2 with CoCr alloy **g** Design-3 with stainless steel alloy **h** Design-3 with titanium alloy **i** Design-3 with CoCr alloy

principal stress for the implant plate is between the moderate and the maximum value but inclined more toward the maximum value which is shown by dark yellow color. From Design-2 with CoCr alloy, it can be observed that the maximum principal stress for the implant plate is between a moderate and the maximum value but inclined more toward the maximum value which is shown by dark yellow color.

From Design-3 with SS316L alloy, it can be observed that the maximum principal stress for the implant plate is inclined more toward the minimum value which is under permissible range and is shown by dark blue color. From Design-3 with titanium alloy, it can be observed that the maximum principal stress for the implant plate is inclined more toward the minimum value which is under permissible range and is shown by dark blue color. From Design-3 with CoCr alloy, it can be observed that the maximum principal stress for the implant plate is more toward the minimum value which is under permissible range and is shown by dark blue color.

After performing analysis on femur bone plate using different materials and different designs, the final results obtained are shown in Table 5.

In Design-1, the maximum principal stress using different material follows a similar kind of pattern. In Design-2, the maximum principal stress values for chromium–cobalt alloys follow a different pattern but for titanium alloy and stainless steel alloy follow similar kind of pattern. In Design-3, the maximum principal stress values for chromium–cobalt alloy follow a different pattern, but for titanium alloy and stainless steel alloy, a similar kind of pattern is observed.

3.4 Fatigue Performance

From Design-1 with SS316L alloy, it can be observed that fatigue performance for an implant plate is more inclined toward the maximum which is shown by dark blue and light blue colors. From Design-1 with titanium alloy, it can be observed that fatigue performance for an implant plate is more toward the maximum which is shown by dark blue and light blue colors. From Design-1 with CoCr alloy, it can be observed that the fatigue performance for the implant plate is variable and at different points on the plate different colors can be observed.

From Design-2 with SS316L alloy, it can be observed that fatigue performance is inclined more toward the maximum which is shown by dark blue and light blue colors. From Design-2 with titanium alloy, it can be observed that fatigue performance for an implant plate is more toward the maximum which is shown by dark blue and light blue colors. From Design-2 with CoCr alloy, it can be observed that fatigue performance for the implant plate is more toward the maximum which is shown by dark blue and light blue colors.

From Design-3 with SS316L alloy, it can be observed that fatigue performance for the implant plate is more toward the maximum which is shown by dark blue and light blue colors. From Design-3 with titanium alloy, it can be observed that fatigue performance for the implant plate is more toward the maximum which is shown by

Table 5 Maximum principal stress

Time	Design-1 SS316L	Design-1 Titanium alloy	Design-1 CoCr alloy	Design-2 SS316L	Design-2 Titanium alloy	Design-2 CoCr alloy	Design-3 SS316L	Design-3 Titanium alloy	Design-3 CoCr alloy
0.1	105.75	99.468	99.468	93.821	67.998	67.998	149.26	98.979	98.979
0.2	240.38	228.91	228.91	648.58	461.46	461.46	311.08	207.58	207.58
0.3	374.8	359.23	359.23	663.09	477.03	477.03	471.91	315.53	315.53
0.4	509.88	490.1	490.1	1741.3	11,321	11,321	632.72	423.45	423.45
0.5	644.99	19,667	19,667	10,935	15,669	15,669	793.56	531.4	531.4
0.6	20,892	33,856	33,856	14,643	21,775	21,775	954.44	639.37	639.37
0.7	36,723	29,565	29,565	65,677	33,273	33,273	1115.3	747.37	747.37
0.8	40,913	70,517	70,517	25,362	33,692	33,692	1276.3	855.4	855.4
0.9	78,315	83,031	83,031	283.64	40,259	40,259	1437.2	963.44	963.44
1	1.03E+05	80,069	80,069	261.61	46,009	46,009	1598.2	1071.5	1071.5

dark blue color. From Design-3 with CoCr alloy, it can be observed that fatigue performance for the implant plate is more toward the maximum which is shown in Fig. 6 by dark blue color.

4 Discussion

The current work involves transient structural analysis on femur bone implant made up of different plates, screws and biomaterials. Conventionally used biomaterials such as stainless steel (SS316L) alloy, Ti alloy (grade-II Ti6A14V) and CoCr alloy are used for all the three assemblies (Design-1, Design-2 and Design-3). All the assemblies are analyzed by finite element method employing transient structural analysis (a tool on ANSYS).

After performing analyses for Design-1 with different biomaterials, total deformation is observed as 4.2439 mm for SS316L and 4.3219 mm for both the alloys (Ti6A14V and CoCr alloy). Similarly, equivalent stress for Design-1 is observed as 895.16 MPa for SS316L and 835.2 MPa for both the alloys (Ti6A14V and CoCr alloy). Also, maximum principal stress for Design-1 is observed as 1032.8 MPa for SS316L and 800.69 MPa for both the alloys (Ti6A14V and CoCr alloy).

After performing analyses for Design-2 with different biomaterials, total deformation is observed as 2.7192 mm for SS316L and 2.8983 mm for both the alloys (Ti6A14V and CoCr alloy). Similarly, equivalent stress for Design-2 is observed as 1093.6 MPa for SS316L and 865.47 MPa for both the alloys (Ti6A14V and CoCr alloy). Also, maximum principal stress for Design-2 is observed as 261.61 MPa for SS316L and 460.09 MPa for both the alloys (Ti6A14V and CoCr alloy).

After performing analyses forDesign-3 with different biomaterials, total deformation is observed as 3.2721 mm for SS316L and 3.3999 mm for both the alloys (Ti6A14V and CoCr alloy). Similarly, equivalent stress for Design-2 is observed as 1657.5 MPa for SS316L and 1028.4 MPa for both the alloys (Ti6A14V and CoCr alloy). Also, maximum principal stress for Design-2 is observed as 1598.2 MPa for SS316L and 1071.5 MPa for both the alloys (Ti6A14V and CoCr alloy).

Based on these observations, a comparison of analyzed data is shown in Fig. 7 which describes the output parametric values vis-a-vis applied input parametric values employing FEM.

5 Conclusion

An implant is one of the most frequently employed medical devices for critical fracture fixation of bones. It consists of the implant plate, screws, etc., and each one of these elements has a specific role to play. It is a fair assumption that an implant plate designed to bear axial compressive load and required to support the longest bone (Femur) will be strong enough to support all other bones in the human body.

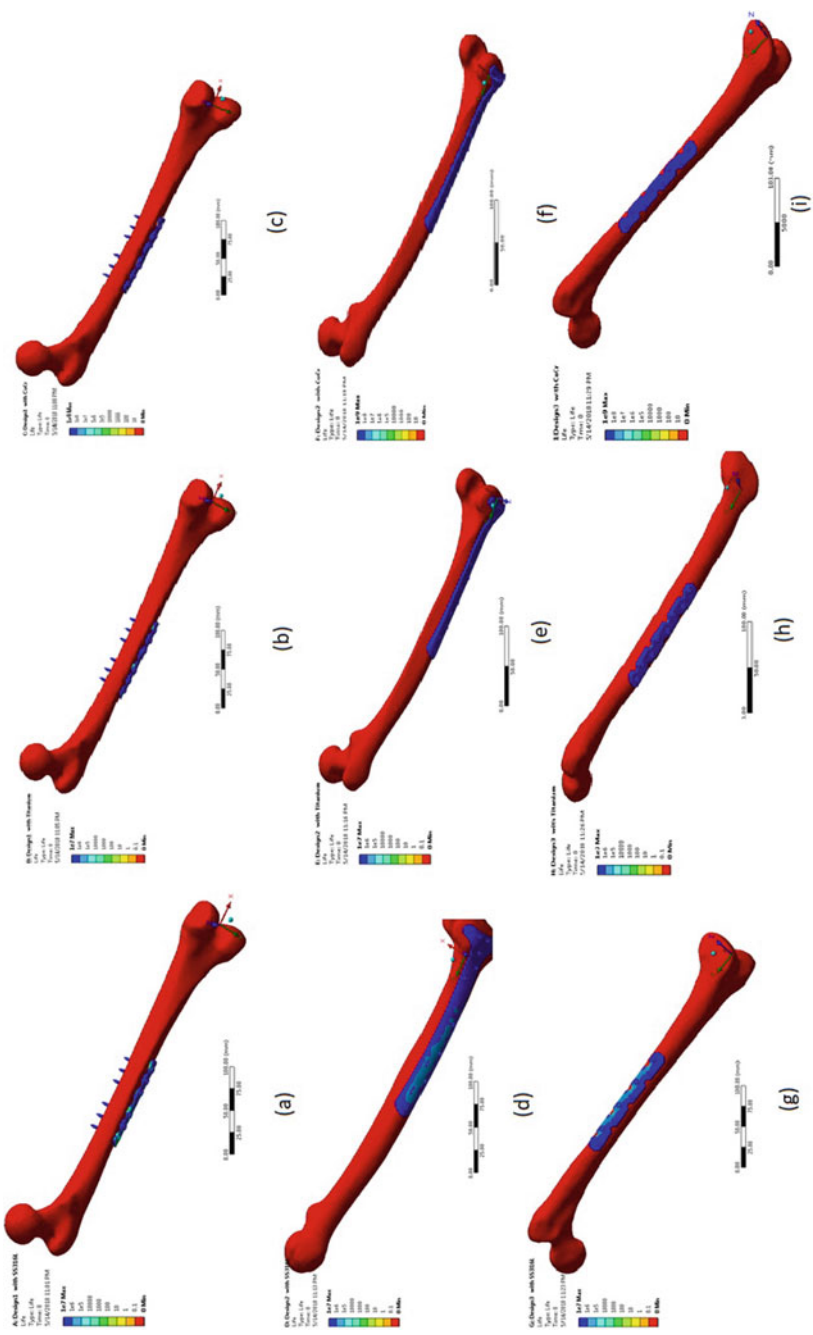

Fig. 6 Fatigue performance of three designs of plate with its correspondingly used materials, i.e., **a** Design-1 with stainless steel alloy **b** Design-1 with titanium alloy **c** Design-1 with CoCr alloy **d** Design-2 with stainless steel alloy **e** Design-2 with titanium alloy **f** Design-2 with CoCr alloy **g** Design-3 with stainless steel alloy **h** Design-3 with titanium alloy **i** Design-3 with CoCr alloy

	Design-1, SS	Design-1, Ti-Alloy	Design-1, Co-Cr	Design-2, SS	Design-2, Ti-alloy	Design-2, Co-Cr	Design-3, SS	Design-3, Ti-alloys	Design-3, Co-Cr
Totoal Deformation (mm)	4.24	4.32	4.32	2.72	2.89	2.8983	3.2721	3.39	3.39
Life Cycle	502.23	144.67	107.5	122.52	419.14	419.14	1222.7	670.82	670.82
Max. principal Stress (Mpa)	1032.8	800.69	800.69	261.61	460.09	460.09	1598.2	1071.5	1071.5
Max. Equivalent Stress (Mpa)	895.16	835.2	835.2	1093.6	865.47	865.47	1657.5	1028.4	1028.4

Fig. 7 Comparatively analyzed data for three design assemblies with each biomaterial

This computational analysis has focused on different designs and different materials for the implant plate subjected to dynamic loading. Structural and fatigue behaviors have been analyzed for the minor single crack in the middle of the femur bone shaft. It is basically observed that out of all materials considered, titanium alloy grade-II has the lowest value of equivalent stress, deformation and maximum principal stress for similar loading conditions. It is precisely because of this that this alloy becomes the preferable choice as it offers good strength, load sustainability and corrosion resistance. Implant plates are immensely useful for orthopedic patients that require appropriate healing of bone over a period of time. However, they may require removal after fulfilling their intended purpose, and this necessitates a secondary surgery. There is tremendous future research potential scope in this area, with adequate focus on the material used, use of biodegradable materials, exhaustive design by incorporating a number of design parameters, some of which may not be getting used at this point, as also analysis relying on implant dissolution rate, rate of corrosion, effect of operating environment, etc.

References

1. Chandra G, Pandey A, Pandey S (2020) Design of a biodegradable plate for femoral shaft fracture fixation. Med Eng Phys 81:86–96. https://doi.org/10.1016/j.medengphy.2020.05.010
2. Chandra G, Pandey A (2020) Biodegradable bone implants in orthopedic applications: a review. Biocybern Biomed Eng 40(2):596–610. https://doi.org/10.1016/j.bbe.2020.02.003
3. Parashar SK, Sharma JK (2016) A review on application of finite element modelling in bone biomechanics. Perspect Sci 8:696–698. https://doi.org/10.1016/j.pisc.2016.06.062
4. Prakash C, Singh S, Verma K, Sidhu SS, Singh S (2018) Synthesis and characterization of Mg–Zn–Mn–HA composite by spark plasma sintering process for orthopedic applications. Vacuum 155(May):578–584. https://doi.org/10.1016/j.vacuum.2018.06.063
5. Satapathy PK, Sahoo B, Panda LN, Das S (2018) Finite element analysis of functionally graded bone plate at femur bone fracture site. IOP Conf Ser Mater Sci Eng 330(1). https://doi.org/10.1088/1757-899X/330/1/012027
6. Kadam AG, Pawar SA, Abhang SA (2017) A review on finite element analysis of different biomaterials used in orthopedic implantation. Int Res J Eng Technol 4(4):2192–2195. Available https://www.irjet.net/archives/V4/i4/IRJET-V4I4559.pdf
7. Xie G, Takada H, Kanetaka H (2016) Development of high performance MgFe alloy as potential biodegradable materials. Mater Sci Eng A 671:48–53. https://doi.org/10.1016/j.msea.2016.06.051
8. Naidubabu Y, Mohana Rao G, Rajasekhar K, Ratna Sunil B (2017) Design and simulation of polymethyl methacrylate-titanium composite bone fixing plates using finite element analysis: optimizing the composition to minimize the stress shielding effect. Proc Inst Mech Eng Part C J Mech Eng Sci 231(23):4402–4412. https://doi.org/10.1177/0954406216668550
9. Dhanopia A, Bhargava M (2017) Finite element analysis of human fractured femur bone implantation with PMMA thermoplastic prosthetic plate. Procedia Eng 173:1658–1665. https://doi.org/10.1016/j.proeng.2016.12.190
10. Phillips ATM, Villette CC, Modenese L (2015) Femoral bone mesoscale structural architecture prediction using musculoskeletal and finite element modelling. Int Biomech 2 (1):43–61. https://doi.org/10.1080/23335432.2015.1017609
11. Ali W, Mehboob A, Han MG, Chang SH (2019) Effect of fluoride coating on degradation behaviour of unidirectional Mg/PLA biodegradable composite for load-bearing bone implant application. Compos Part A Appl Sci Manuf 124. https://doi.org/10.1016/j.compositesa.2019.05.032
12. Sanchez AHM, Luthringer BJC, Feyerabend F, Willumeit R (2015) Mg and Mg alloys: how comparable are in vitro and in vivo corrosion rates? A review. Acta Biomater 13:16–31. https://doi.org/10.1016/j.actbio.2014.11.048
13. Qasim M et al (2016) Patient-specific finite element estimated femur strength as a predictor of the risk of hip fracture: the effect of methodological determinants. Osteoporos Int 27(9):2815–2822. https://doi.org/10.1007/s00198-016-3597-4
14. Chandra G, Pandey A (2020) Preparation strategies for Mg-alloys for biodegradable orthopaedic implants and other biomedical applications: a review. IRBM 1:1–21. https://doi.org/10.1016/j.irbm.2020.06.003
15. Zheng YF, Gu XN, Witte F (2014) Biodegradable metals. Mater Sci Eng R Reports 77:1–34. https://doi.org/10.1016/j.mser.2014.01.001
16. Gu X et al (2018) In vitro and in vivo studies on as-extruded Mg—5.25wt.%Zn—0.6wt.%Ca alloy as biodegradable metal. Sci China Mater 61(4):619–628. https://doi.org/10.1007/s40843-017-9205-x
17. Yao H, Wen J, Xiong Y, Lu Y, Ren F, Cao W (2018) Extrusion temperature impacts on biometallic Mg–2.0Zn–0.5Zr–3.0Gd (wt%) solid-solution alloy. J Alloys Compd 739:468–480. https://doi.org/10.1016/j.jallcom.2017.12.225
18. Zakiuddin KS, Khan IA, Hinge RA (2016) Review paper on biomechanical analysis of human femur. Int J Innov Res Sci Eng 2:356–363

19. Zhang S et al (2010) Research on an Mg–Zn alloy as a degradable biomaterial. Acta Biomater 6(2):626–640. https://doi.org/10.1016/j.actbio.2009.06.028
20. Razzaghi M, Kasiri-Asgarani M, Bakhsheshi-Rad HR, Ghayour H (2020) Microstructure, mechanical properties, and in-vitro biocompatibility of nano-NiTi reinforced Mg–3Zn–0.5Ag alloy: prepared by mechanical alloying for implant applications. Compos Part B Eng 190:107947. https://doi.org/10.1016/j.compositesb.2020.107947
21. Vignoli LL, Kenedi PP (2016) Bone anisotropy—analytical and finite element analysis. Lat Am J Solids Struct 13(1):51–72. https://doi.org/10.1590/1679-78251814
22. Sheikh MS, Ganorkar AP (2015) Optimization of femoral intramedullary nailing using finite element analysis. 2(4):123–125